Journal of King Saud University – Science 32 (2020) 1612–1618

Contents lists available at ScienceDirect

Journal of King Saud University – Science

journal homepage: www.sciencedirect.com

Original article

# Equilibrium synthesis and magnetic properties of $BaFe_{12}O_{19}/NiFe_2O_4$ nanocomposite prepared by co precipitation method

C. Thirupathy [a], S. Cathrin Lims [a], S. John Sundaram [a,*], Ahmed Hossam Mahmoud [b], K. Kaviyarasu [c,d]

[a] Department of Physics, Sacred Heart College (Autonomous), Tirupattur - 635601, Tirupattur District, Tamil Nadu, India
[b] Department of Zoology, College of Science, King Saud University, Riyadh, Saudi Arabia
[c] UNESCO-UNISA Africa Chair in Nanosciences/Nanotechnology Laboratories, College of Graduate Studies, University of South Africa (UNISA), Muckleneuk Ridge, PO Box 392, Pretoria, South Africa
[d] Nanosciences African Network (NANOAFNET), Materials Research Group (MRG), iThemba LABS-National Research Foundation (NRF), 1 Old Faure Road, 7129, PO Box 722, Somerset West, Western Cape Province, South Africa

ARTICLE INFO

*Article history:*
Received 30 September 2019
Revised 8 December 2019
Accepted 17 December 2019
Available online 27 December 2019

*Keywords:*
Magnetic properties
Electron microscopy
Ferrite materials
UV–vis absorbance spectroscopy
XRD phase transition

ABSTRACT

The hard and soft magnetic nanocomposites ($BaFe_{12}O_{19}/NiFe_2O_4$) at the ratio 1:1 were prepared by simple mixing and heat treatment. XRD peak indicates the formation of good crystalline quality of the prepared sample. The FTIR spectra reveals the bands for metal oxygen stretching which ranges from 584 $cm^{-1}$ to 540 $cm^{-1}$ forms the tetrahedral shape in nature. However, the hexaferrite site ranges from 580 $cm^{-1}$ to 440 $cm^{-1}$ and this bands assign to Ba-O and Fe-O bonds respectively. Furthermore, the UV–visible range, the observed absorption peak indicates that the prepared sample color is congo red, the characteristic absorption peaks at ~739 nm for $BaFe_{12}O_{19}$, 698 nm for $NiFe_2O_4$ and 780 nm for $BaFe_{12}O_{19}/NiFe_2O_4$. Overall, the ferrite powder seems agglomerated, but the microstructure shows its respective structure. The particle size of $BaFe_{12}O_{19}$ (hexagonal) is 150 nm, again the particle size of $NiFe_2O_4$ (cubic) is 89 nm apparently. Finally, the structure of composite ($BaFe_{12}O_{19}/NiFe_2O_4$) material seems to achieve intermediate and its particle size is 120 nm correspondingly.


## 1. Introduction

Ferrites have numerous industrial applications with excellent electric and magnetic properties (Zhidong et al., 2006), which shows promising properties in radar absorption, microwave absorption, magneto optic or perpendicular recording media, magnetic device, transformers and spintronics (Remya et al., 2016). Therefore, the magnetic nanocomposites have obvious advantage over nonmagnetic materials, these nanocomposite materials consist of hard and soft magnetic phase (Prakash et al., 2016). Which make them suitable for many different applications which include permanent magnet too (Kadi and Mohamed, 2014). The magnetic fillers of ferrite materials are spinal ferrite and hexaferrite it shows a loss nearer to dipole relaxation and ferromagnetic resonance (Couture et al., 2017). In addition, spinal ferrites can be used in EMR absorption upto 3 GHz frequency range, but hexagonal ferrite use up to the frequency range of (2–18 GHz) because of uniaxial anisotropic property (Sun et al., 2017). Hexaferrites are sub classified in different categories M,U,W,X,Y and Z with general formula like $BaFe_{12}O_{19}$; $Ba_4Me_2Fe_{36}O_{60}$; $BaMe_2Fe_{16}O_{22}$; $Ba_2Me_2Fe_{28}O_{46}$; $BaMe_2Fe_{12}O_{22}$ and $Ba_2Me_2Fe_2O_{41}$. Where Me- divalent cation of first transition series like Ni, Co, Zn and Mg. Among different system these combing hexagonal ferrite with spinal/inverse spinal ferrite have obtained noticeable attention by researcher (Bashir et al., 2019a). In order to get high crystalline mono-domain particle barium hexaferrite and nickel ferrite different synthesis techniques were adapted they are sol–gel (Bashir et al., 2019b), co-precipitation (Williams et al., 2018), solvothermal method (Tyagi et al., 2018), organic acid precursor method (Ali et al., 2017) etc., In this work the present investigation deals with barium and nickel ferrite nanocomposite followed by co-precipitation method. Due to this method is low cost and easytechnique to mass production compared with other applications (Kennedy et al., 2016). Therefore, the established nanocomposites were characterized by X-ray diffraction (XRD) pattern will reveal the crystalline nature

* Corresponding author.
*E-mail address:* johnsundaram@shctpt.edu (S. John Sundaram).
Peer review under responsibility of King Saud University.

Production and hosting by Elsevier

https://doi.org/10.1016/j.jksus.2019.12.019
1018-3647/

of nanocomposites. FTIR spectrum shows the presence of functional group and vibrational bands at the surface of BaFe12O19 / NiFe2O4 nanocomposite. Finally, scanning electron microscopy (SEM) shows the morphology growth of the samples with EDAX will explain to confirm the elemental composition which is present in the compound. Lastly, VSM will show the magnetic property of the entire samples were reported in detail.

## 2. Experimental procedure

### *2.1. Synthesis of $BaFe_{12}O_{19}/NiFe_2O_4$ and $BaFe_{12}O_{19}$ /$NiFe_2O_4$ nanocomposites*

In the present investigation barium nitrate($Ba(No_3)_2$), ferric nitrate monohydrate ($(FeH_{18}N_3O_{18})_{12}$; nickel nitrate ($Ni(No_3)_2$) and ammonia solution is used for synthesizing $BaFe_{12}O_{19}/NiFe_2O_4$ and $BaFe_{12}O_{19}/NiFe_2O_4$nanocomposite by co-precipitation method.1% of barium nitrate and 12% of ferric nitrate monohydrate of molecular weight is taken (I). The, 1% nickel nitrate and 2% of ferric nitrate monohydrate of molecular weight taken (II) separately. Add the two mixture separately in a 50 ml of water, let these mixtures stir for 2 h continuously until the compound's mixtures and dissolves completely. In that condition, after 2 h ammonia solution was added drop by drop until the precipitate forms then allowed to stir for an hour, finally, the brown precipitate deposits at the bottom and the crystal-clear liquid will deposits on the brown precipitate. Then the solution is completely washed with water and ethanol for several times, the washed nanoparticles were kept in hot air oven for 24 h at 120 °C. The dried, brown rocky like nanomaterial forms. By using the mortar, the brown rocky material was grained well. The grinded particles were put into a silicon crucible kept in a muffled furnace for 2 h up to 800 °C. Therefore, the prepared $BaFe_{12}O_{19}$and $NiFe_2O_4$nanoparticles has been done by mixing the hard and soft ferrite in weight ratio of 1:1then the sample was grained and heated for 100 °C respectively.

## 3. Results and discussion

### *3.1. X-ray powder diffraction (XRD)*

The XRD pattern of barium hexaferrite ($BaFe_{12}O_{19}$) and nickel ferrite ($NiFe_2O_4$) nanopowders were calcinated under 800 °C for 2 h as shown in Fig. 1.The hard and soft magnetic nanocomposites ($BaFe_{12}O_{19}/NiFe_2O_4$)at the ratio 1:1 were prepared by simple mixing and heat treatment. The well-defined sharp peak indicates the formation of good crystalline quality of the prepared sample. The peaks in $BaFe_{12}O_{19}$ corresponds to hexagonal structure (a = b ≠ c) according to the (JCPDS file number 84–0757) and $NiFe_2O_4$ corresponds to cubic structure (a = b = c) according to (JCPDS file number 86–2267). All these diffraction peaks for $BaFe_{12}O_{19}$ (♣) and $NiFe_2O_4$ (◆) and no other impurity peaks has been observed even after simple mixing heat treatment. Therefore, the XRDpeak positions of those composites $BaFe_{12}O_{19}/NiFe_2O_4$ has both hard and soft magnetic ferrite phase and this confirms the presence of both $BaFe_{12}O_{19}$ and $NiFe_2O_4$ exist in nature (Kaviyarasu et al., 2012). The average grain size of powder sample was estimated from full width at half maximum (FWHM) by using Debye Scherer formula to determine the crystallite size, dislocation, lattice strain and inter planner distance were listed in Table 1.

### *3.2. Fourier transform infra-red spectroscopy (FTIR)*

The FTIR spectra were recorded in mid-range 400 $cm^{-1}$ to 4000 $cm^{-1}$for barium hexaferrite ($BaFe_{12}O_{19}$) and nickel ferrite ($NiFe_2O_4$) and the composite of $BaFe_{12}O_{19}/NiFe_2O_4$ with the ratio 1:1 as shown in the Fig. 2. The FTIR spectra reveals the bands for metal oxygen stretching which ranges from 584 $cm^{-1}$ to

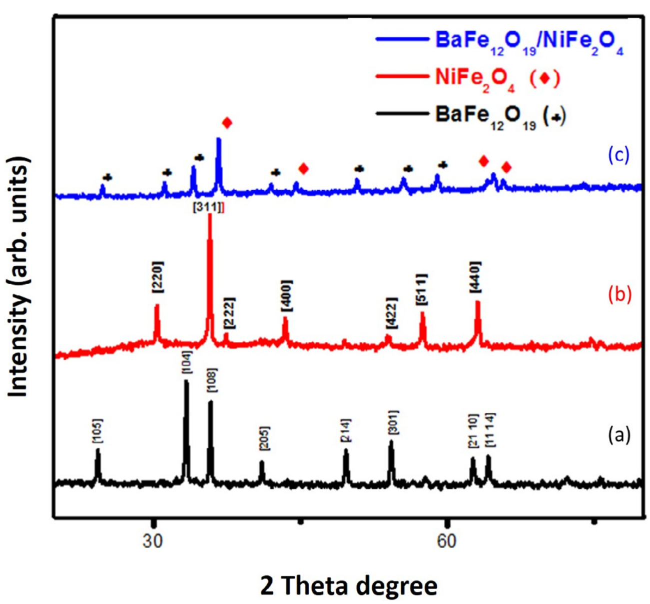


**Fig. 1.** XRD pattern of (a) $BaFe_{12}O_{19}$; (b) $NiFe_2O_4$ and (c) $BaFe_{12}O_{19}/NiFe_2O_4$.

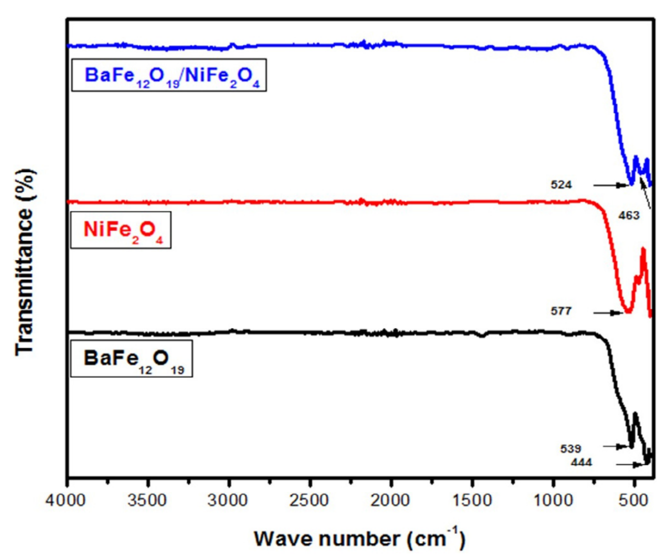


**Fig. 2.** FTIR spectrum of $BaFe_{12}O_{19}$; $NiFe_2O_4$ and$BaFe_{12}O_{19}/NiFe_2O_4$.

**Table 1**
Powder XRD pattern of (a) $BaFe_{12}O_{19}$, (b) $NiFe_2O_4$ and (c) $BaFe_{12}O_{19}/NiFe_2O_4$.

| Sample | $BaFe_{12}O_{19}$ | $NiFe_2O_4$ | $BaFe_{12}O_{19}/NiFe_2O_4$ |
|---|---|---|---|
| Crystallite size | 41 nm | 40 nm | 31 nm |
| Dislocation $(\delta) = \frac{1}{L2}$ | $0.493 \times 10^{15}$ | $0.625 \times 10^{15}$ | $1.040 \times 10^{15}$ |
| Lattice train$(\sum) = \frac{\beta COS\theta}{4}$ | $0.9371 \times 10^{-3}$ | $0.9935 \times 10^{-3}$ | $1.0891 \times 10^{-3}$ |
| Inter planner distance($\mathbf{d}$) | $0.952 \times 10^{10}$ | $0.921 \times 10^{10}$ | $2.0033 \times 10^{10}$ |

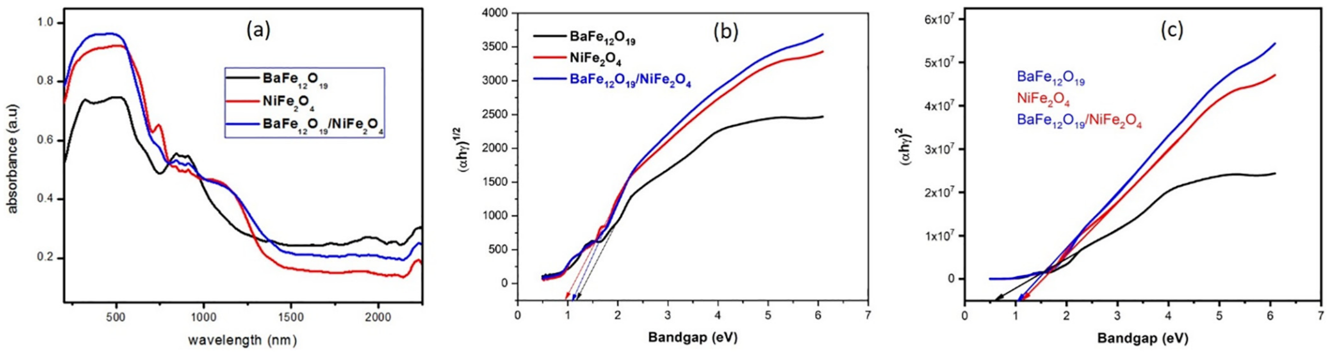


**Fig. 3.** (a) UV–visible spectrum of $BaFe_{12}O_{19}$, $NiFe_2O_4$,$BaFe_{12}O_{19}/NiFe_2O_4$nanocomposites, (b) Tauc plot forindirect transition, (c) direct transition.

**Table 2**
Tauc plot of $BaFe_{12}O_{19}$;$NiFe_2O_4$ and $BaFe_{12}O_{19}/NiFe_2O_4$nanocomposites for (a) direct transition, (b) indirect transition.

| Sample | Direct bandgap energy (eV) | Indirect bandgap energy (eV) |
|---|---|---|
| $BaFe_{12}O_{19}$ | 1.72 | 1.41 |
| $NiFe_2O_4$ | 1.40 | 1.16 |
| $BaFe_{12}O_{19}/NiFe_2O_4$ | 1.57 | 1.05 |

540 $cm^{-1}$ forms the tetrahedral shape. The hexaferrite site ranges from 580 $cm^{-1}$ to 440 $cm^{-1}$ and this bands assign to Ba-O and Fe-O bonds. The other bands like$Co_2$-, –OH peaks are completely vanished under calcination at 800 °C for 2 h.

### 3.3. UV–visible spectrometer

The optical properties are closely related to the atomic structure, electronic bond patterns. The optical properties of nano

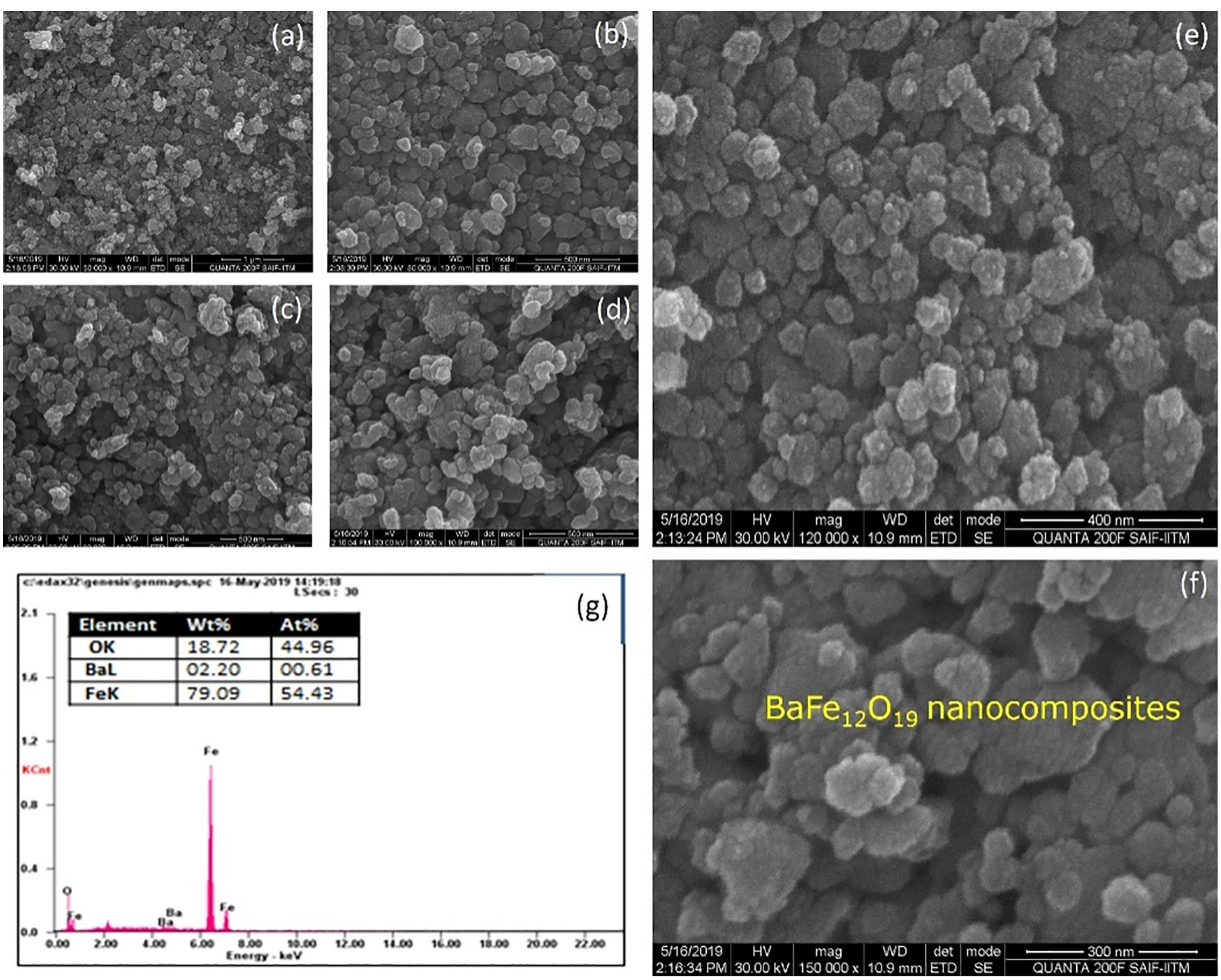


**Fig. 4.** (a-g). SEM with EDAX image for $BaFe_{12}O_{19}$ nanocomposites.

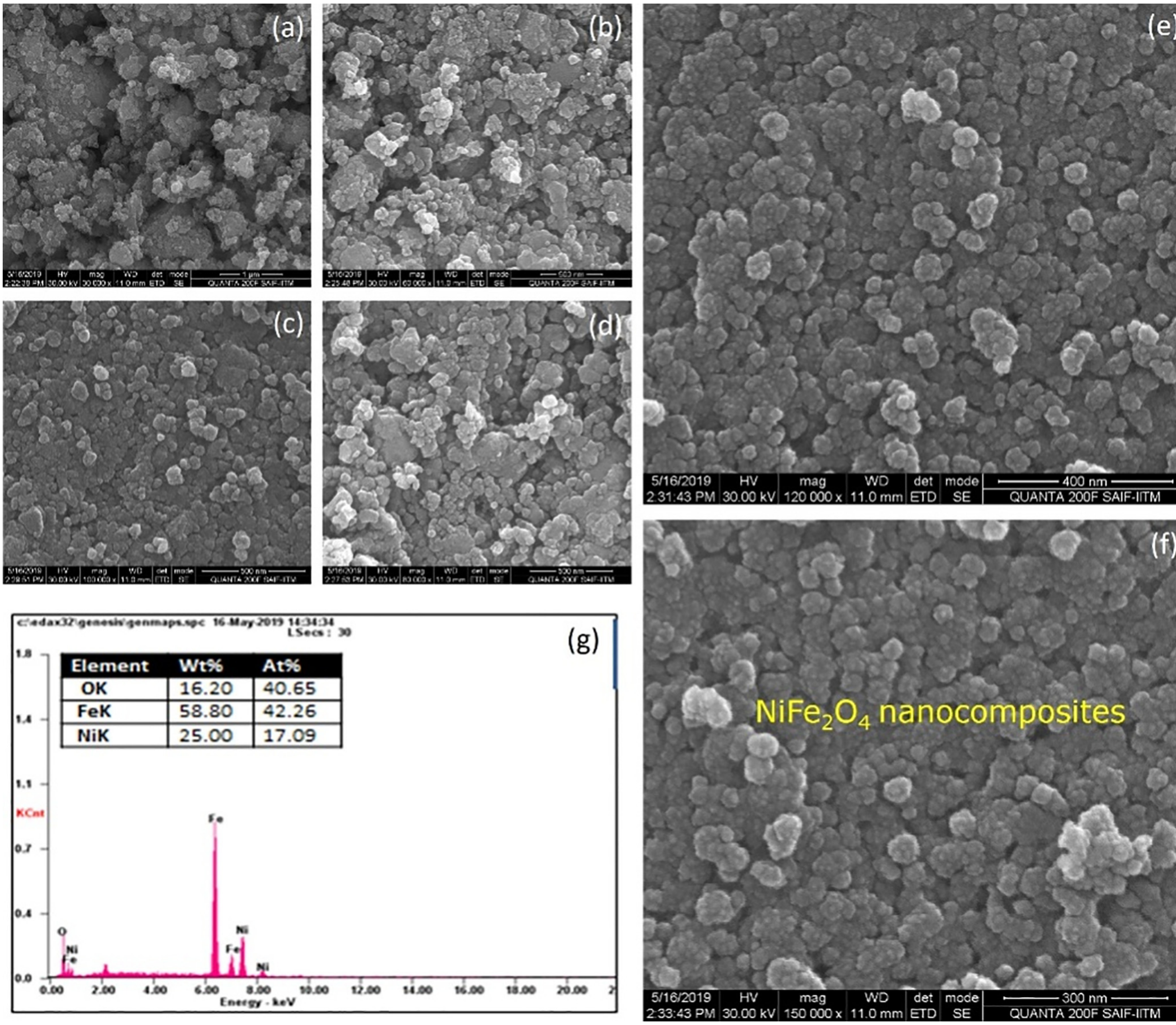


**Fig. 5.** (a-g). SEM with EDAX image for$NiFe_2O_4$ nanocomposites.

composites were analyzed from wavelength ranges from 200 to 2500 nm as shown in Fig. 3(a).At UV–visible range the observed absorption peak indicates that the prepared sample color is congo red, the characteristic absorption peaks at ~739 nm for $BaFe_{12}O_{19}$; 698 nm for $NiFe_2O_4$ and 780 nm for $BaFe_{12}O_{19}/NiFe_2O_4$ (MobeenAmanulla et al., 2018). Therefore, the energy gap can be obtained from *Tauc plot*, $\alpha h\gamma = A(h\gamma - Eg)^m$; where, $\alpha$ – is the absorption co-efficient; $h\gamma$ - is photon energy; $E_g$ - is the optical energy band gap; A – is a constant; M – is the characteristics of transition. At near infrared range transmittance occurred so the material can be used in radar absorption or microwave absorption applications (Kaviyarasu et al., 2017). The energy gap can be obtained from *Tauc plot* as shown in Fig. 3(b, c). The *Tauc plots* were plotted for direct and indirect transition and the band gap were listed in the Table2.

### 3.4. Scanning electron microscope& EDAX

The scanning electron microscopic image $BaFe_{12}O_{19}$, $NiFe_2O_4$-ferrite nanoparticles as well as hard and soft magnetic phase mixed ($BaFe_{12}O_{19}/NiFe_2O_4$) in the ratio of 1:1 as shown in the Figs. 4–6, the image says that the ferrites and composites are not well dispersed because of its un favorable condition (Kaviyarasu et al., 2013). Ferrite powder seems agglomerated but the micro structure shows its respective structure (Sazelee et al., 2018). The particle size of $BaFe_{12}O_{19}$ (hexagonal) is 150 nm as shown in Fig. 4(a-g), the particle size of $NiFe_2O_4$(cubic) is 89 nm as shown in Fig. 5(a-g) and the structure of composite ($BaFe_{12}O_{19}/NiFe_2O_{4)}$ material seems to achieve intermediate and its particle size of is 120 nm Fig. 6(a-g). From the image the elongated shape says that the composition is insufficient to the formation of nanoparticles (Salwa et al., 2014). The spherical particles will also disappear by increasing its temperature (Jesudoss et al., 2017). The data which is generated by energy dispersive X-ray microanalysis has some peaks corresponds to different elements that are present in the sample and each element has a specific peak of unique energy, all comprehensively documented (Ming and Liang Gao, 2012). The EDAX spectra of $BaFe_{12}O_{19}$; $NiFe_2O_4$ and $BaFe_{12}O_{19}/NiFe_2O_4$ as shown in Fig. 6, the peak corresponding to the elements BA, Ni, Fe and O were observed in ferrite nano particles and the peaks of the elements Ba, Ni, Fe and O were observed in composite (Virk et al., 2011). The observed percentage of Ba, Ni, Fe and O match with

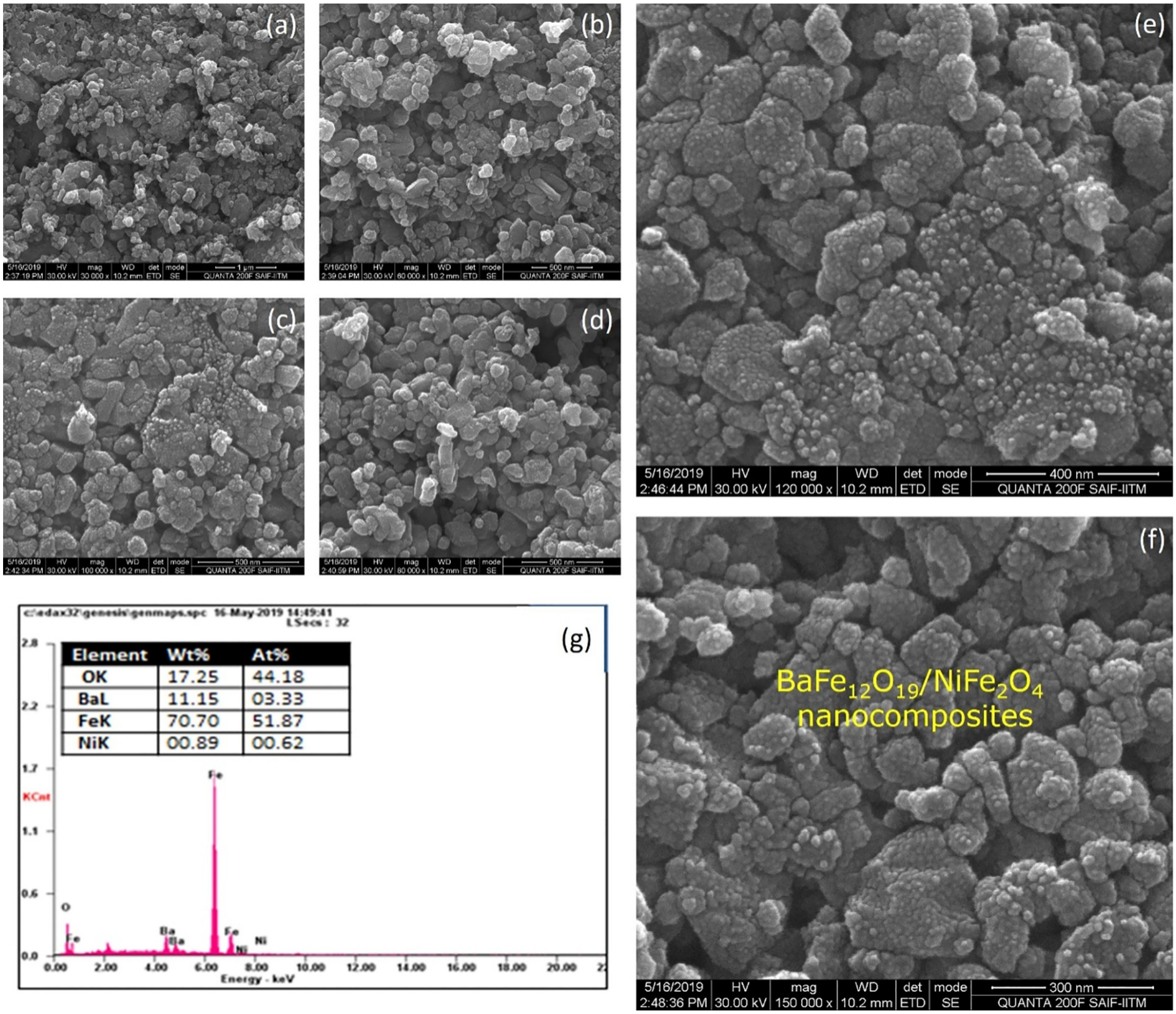


**Fig. 6.** (a-g). SEM with EDAX image for$BaFe_{12}O_{19}/NiFe_2O_4$nanocomposites.

**Table 3**
VSM image of $BaFe_{12}O_{19}$, $NiFe_2O_4$ and $BaFe_{12}O_{19}/NiFe_2O_4$nanocomposites.

| S. No | Properties | $BaFe_{12}O_{19}$ | $NiFe_2O_4$ | $Ba_2Ni_2Fe_{12}O_{22}$ |
|---|---|---|---|---|
| 1 | Coercivity (Hci) | 6246.3 G | 190.93 G | 824.04 G |
| 2 | Saturation Magnetization (Ms) | 0.41713 emu | 0.21146 emu | 0.38348 emu |
| 3 | Retentivity (Mr) | 0.19876 emu | $48.071E^{-3}$ emu | 0.12533 emu |

the amount of respective precursor without any characteristic peak (Gurbuz et al., 2012). The atomic percentage and weight percentage were also listed.

### 3.5. Vibrating sample magnetometer (VSM)

The magnetic properties were studied using vibrating sample magnetometer at room temperature and various magnetic properties were listed using the curve below in the Table 3 (Sivakumara et al., 2012). Hysteresis loop are important in the construction of several electrical devices as shown in Fig. 7(a-d).

## 4. Conclusion

In summary, the structure of nanocomposites $BaFe_{12}O_{19}/NiFe_2O_4$seems to achieve intermediate and its particle size of is 120 nm. From the XRD peak positions have confirmed the presence of both $BaFe_{12}O_{19}$ and $NiFe_2O_4$ exist in the composites. The FTIR spectra reveals the bands for metal oxygen stretching which ranges from 584 $cm^{-1}$ to 540 $cm^{-1}$ and the other bands like $Co_2$–, –OH peaks were completely vanished under calcination at 800 °C for 2 h. SEM image were elongated shapes that the composition is insufficient to the formation of nanoparticles. Therefore, the spherical particles have disappeared by increasing the temperature.

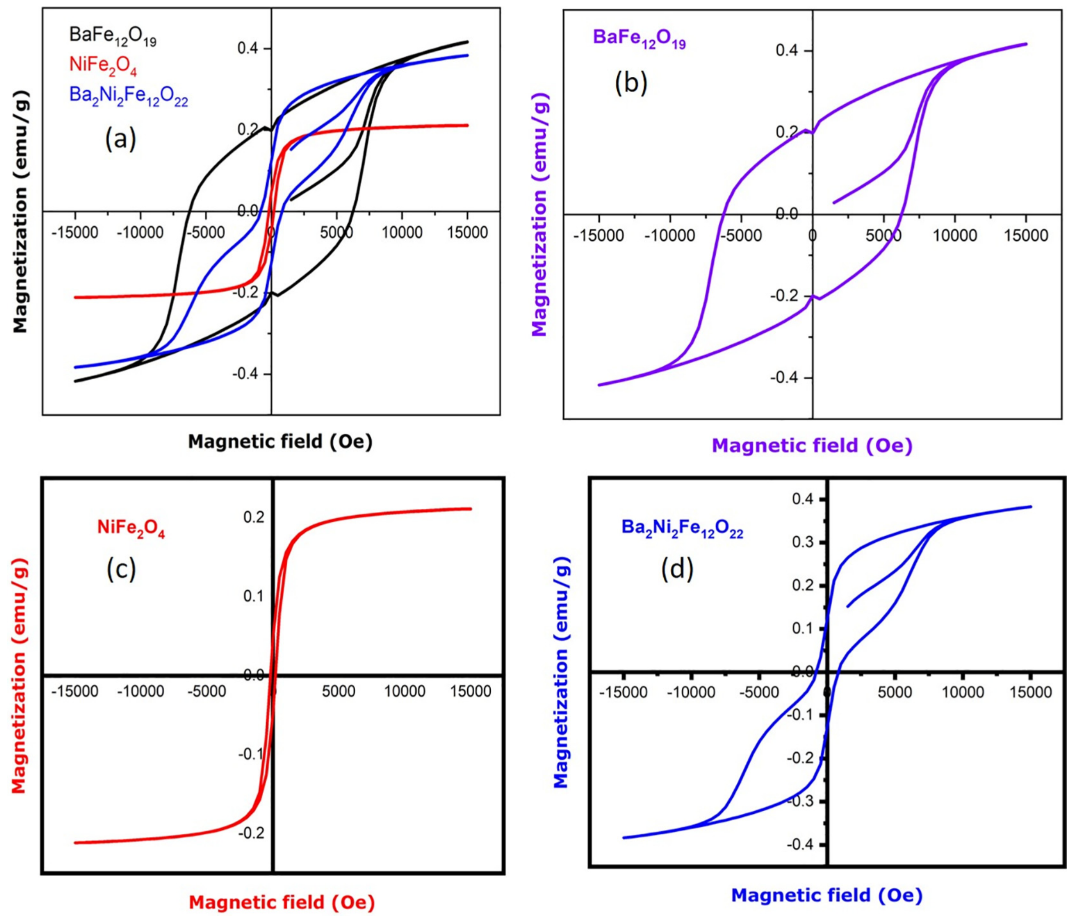


**Fig. 7.** (a) VSM image of different nanocomposites; (b) $BaFe_{12}O_{19}$; (c) $NiFe_2O_4$; (d) $BaFe_{12}O_{19}/NiFe_2O_4$ nanostructures.


## Acknowledgment

The authors extend their appreciation to The Researchers supporting project number (RSP-2019/108) King Saud University, Riyadh, Saudi Arabia.


## References


Ali, K., Bahadur, A., Jabbar, A., Iqbal, S., Imran Bashir, M., Synthesis, Structural, 2017. Dielectric and Magnetic properties of $CuFe_2O_4/MnO_2$ Nanocomposites. J. Magn. Magn. Mater. 434, 30–36.

Bashir, A.K.H., Furqan, C.M., Bharuth-Ram, K., Kaviyarasu, K., Tchokonte, M.B.T., Maaza, M., 2019a. Structural, optical and Mossbauer investigation on the biosynthesized $\alpha$-$Fe_2O_3$: study on different precursors. Physica E 111, 152–157.

Bashir, A.K.H., Razanamahandry, L.C., Nwanya, A.C., Kaviyarasu, K., Saban, W., Mohamed, H.E.A., Nwtampe, S.C., Ezema, F.I., Maaza, M., 2019b. Biosynthesis of NiO nanoparticles for photodegradation of free cyanide solutions under ultraviolet light. J. Phys. Chem. Solids 134, 133–140.

Couture, P., Williams, G.V.M., Kennedy, J., Leveneur, J., Murmu, P.P., Chong, S.V., Rubanov, S., 2017. Nanocrystalline multiferroic $BiFeO_3$ thin films made by room temperature sputtering and thermal annealing, and formation of an iron oxide-induced exchange bias. J. Alloy. Compd. 695, 3061–3068.

Gurbuz, A., Omar, N., Ozdemir, I., CahitKaronglanli, A., Celik, E., 2012. Structural, Thermal and Magnetic properties of Nerium- ferrite powders substituted with Mn, Cu or Co and X (X= Sr and Ni) prepared by the Sol-Gel method. Mater. Technol. 46 (3), 305–310.

Jesudoss, S.K., Judith Vijaya, J., IyyappaRajan, P., Kaviyarasu, K., Sivachidambaram, M., John Kennedy, L., Al-Lohedan, Hamad A., Jothiramalingam, R., Munusamy, Murugan A., 2017. High performance multifunctional green $Co_3O_4$ spinel nanoparticles: photodegradation of textile dye effluents, catalytic hydrogenation of nitro-aromatics and antibacterial potential. Photochem. Photobiol. Sci. 16, 766–778.

Kadi, M.W., Mohamed, R.M., 2014. Synthesis and optimization of cubic $NiFe_2O_4$ nanoparticles with enhanced saturation magnetization. Ceram. Int. 40, 227–232.

Kaviyarasu, K., Raja, A., Devarajan, P.A., 2013. Structural elucidation and spectral characterizations of $Co_3O_4$ nanoflakes. Spectrochim. Acta Part A Mol. Biomol. Spectrosc. 114, 586–591.

Kaviyarasu, K., Devarajan, P.A., Xavier, S.J., Thomas, S.A., Selvakumar, S., 2012. One pot synthesis and characterization of cesium doped $SnO_2$ nanocrystals via a hydrothermal process. J. Mater. Sci. Technol. 28, 15–20.

Kaviyarasu, K., Murmu, P.P., Kennedy, J., Thema, F.T., Letsholathebe, D., Kotsedi, L., Maaza, M., 2017. Structural, optical and magnetic investigation of Gd implanted $CeO_2$ nanocrystals. Nucl. Instrum. Methods Phys. Res., Sect. B 409, 147–152.

Kennedy, J., Murmu, P.P., Leveneur, J., Markwitz, A., Futter, J., 2016. Controlling preferred orientation and electrical conductivity of zinc oxide thin films by post growth annealing treatment. Appl. Surf. Sci. 367, 52–58.

Ming, Liu X., Liang Gao, W., 2012. Preparation and Magnetic Properties of $NiFe_2O_4$ Nanoparticles by Modified Pechini Method, Journal. Mater. Manuf. Processes 27, 905–909.

MobeenAmanulla, A., Jasmine Shahina, S.K., Sundaram, R., Maria Magdalane, C., Kaviyarasu, K., Letsholathebe, D., Mohamed, S.B., Kennedy, J., Maaza, M., 2018. Antibacterial magnetic, optical and humidity sensor studies of $\beta$-$CoMoO_4$-$Co_3O_4$ nanocomposites and its synthesis and characterization. J. Photochem. Photobiol., B 183, 233–241.

Prakash, T., Williams, Grant V.M., Kennedy, J., Rubanov, S., 2016. Formation of magnetic nanoparticles by low energy dual implantation of Ni and Fe into $SiO_2$. J. Alloy. Compd. 667, 255–261.

Remya, K.P., Prabhu, D., Amirthapandian, S., Viswanathan, C., Ponpandian, N., 2016. Exchange spring magnetic behavior in $BaFe_{12}O_{19}/Fe_3O$ nanocomposites. J. Magn. Magn. Mater. 406, 233–238.

Salwa, A.M., Abdel Hameed, M., Ibrahim, M., Nehal, A., 2014. Utilization of iron oxide bearing pellets waste for preparing hard and soft ferromagnetic glass ceramics. J. Adv. Ceram. 3 (4), 259–268.

Sazelee, N.A., Idris, N.H., Md Din, M.F., Mustafa, N.S., Ali, N., Yahya, M.S., Halim Yap, F.A., Sulaiman, N.N., Ismail, M., 2018. Synthesis of $BaFe_{12}O_{19}$ by solid state method and its effect on hydrogen storage properties of $MgH_2$. Int. J. Hydrogen Energy 43, 20853–20860.

Sivakumara, P., Ramesh, R., Ramanand, A., Ponnusamy, S., Muthamizhchelvan, C., 2012. Preparation and properties of nickel ferrite ($NiFe_2O_4$) nanoparticles via sol-gel auto-combustion method. Mater. Res. Bull. 46, 2204–2207.

Sun, L., Zhang, Z., Wang, L., Ju, E., Cao, Y., 2017. Zhang, Structural, dielectric and magnetic properties of $NiFe_2O$ prepared via sol-gel auto-combustion method. J. Magn. Magn. Mater. 421, 65–70.

Tyagi, S., Pandey, V.S., Goel, S., Garg, A., 2018. Synthesis and characterization of RADAR absorbing $BaFe_{12}O_{19}/NiFe_2O_4$ magnetic nanocomposite. Integr. Ferroelectr. 186, 25–31.

Virk, H.S., Sharma, P., Jotania, R., 2011. Comparative study of Ba-M Hexaferrite particles prepared using Microemulsion processing and Co-Precipitation techniques. Int. J. Adv. Eng. Technol. 2, 131–143.

Williams, G.V.M., Prakash, T., Kennedy, J., Chong, S.V., Rubanov, S., 2018. Spin-dependent tunnelling in magnetite nanoparticles. J. Magn. Magn. Mater. 460, 229–233.

Zhidong, H., Limin, D., Dawei, Z., Ze, W., Xianyou, Z., 2006. Synthesis of $BaFe_{12}O_{19}/MFe_2O_4$ (M=Co, Mn) by sol-gel method. Rare Met. 25, 462–465.